Applied Catalysis B: Environment and Energy 346 (2024) 123678

Contents lists available at ScienceDirect

Applied Catalysis B: Environment and Energy

journal homepage: www.elsevier.com/locate/apcatb

Towards high performance durable ceramic fuel cells using a triple conducting perovskite cathode

Zhipeng Liu [a], Heping Xie [a], Yuan Zhang [a,b,**], Junbiao Li [a], Junda You [a], Hongxin Yang [a], Haojie Zhu [a], Meng Ni [b,*], Zongping Shao [c], Bin Chen [a,*]

[a] Guangdong Provincial Key Laboratory of Deep Earth Sciences and Geothermal Energy Exploitation and Utilization, Institute of Deep Earth Sciences and Green Energy, Shenzhen University, Shenzhen 518060, China

[b] Department of Building and Real Estate, Research Institute for Sustainable Urban Development (RISUD) and Research Institute for Smart Energy (RISE), The Hong Kong Polytechnic University, Hung Hom, Kowloon, Hong Kong, China

[c] WA School of Mines: Minerals, Energy and Chemical Engineering, Curtin University, Perth, Western Australia 6845, Australia

ARTICLE INFO

Keywords:
Proton conducting fuel cells
Cathode
Perovskite
Triple conducting
Nb doping

ABSTRACT

To guarantee the efficient and durable operation of oxygen ion/proton-conducting ceramic fuel cells, the cathode materials need to be versatile in terms of high activity, good CO_2 resistance, and matched thermal expansion behavior with electrolyte, etc. In this study, we substituted 10% Nb to the B-site of parent perovskite-$BaCo_{0.7}Fe_{0.2}Y_{0.1}O_{3-\delta}$, to form a single-phase material with triple conducting ($H^+/O^{2-}/e^-$) capability as a highly ORR-active cathode. The doped $BaCo_{0.6}Fe_{0.2}Y_{0.1}Nb_{0.1}O_{3-\delta}$ (BCFYN) shows promising ORR activity due to the optimized oxygen vacancy, improved hydration capacity, and accelerated charge transfer kinetics. The reduction of thermal expansion coefficient (TEC) and enhanced CO_2 resistance also facilitate the cathode durability. As a result, the area-specific resistances of BCFYN electrode at 550 °C for oxygen-ion and proton conducting symmetrical cells were only 0.106 and 0.24 Ω cm^2, respectively. These results indicate that BCFYN is a highly promising cathode material for both SOFCs and PCFCs.

1. Introduction

With the increasing attention to global warming and sustainability, solid oxide fuel cells (SOFCs) have attracted significant interest as the next-generation power generation technology due to their high efficiency in converting fuel energy to electricity without emitting pollutants. Currently, its commercialization still faces challenges in durability and cost due to the relatively high operating temperature (700–800 ℃), which causes issues including material degradation, high manufacturing costs, stack sealing problems, etc [1,2]. Lowering the operating temperature of SOFCs can significantly mitigate those issues and facilitates the commercialization of SOFCs. However, the shift towards intermediate-temperature (<600 ℃) development in SOFCs poses challenges to the activity of the cathode and the ion conductivity of the electrolyte. Using proton conducting electrolytes such as Barium cerates/zirconates Ba(Ce, Zr)O_3 has attracted much attention due to their higher conductivity at low temperatures than traditional oxygen ion electrolyte [3]. Regarding the cathode, the development of high-performance cathodes with low area-specific resistance (ASR), strong CO_2 resistance, and low thermal expansion coefficient at intermediate temperatures becomes crucial. Traditional cathode materials, such as $La_{0.8}Sr_{0.2}MnO_3$ (LSM), are pure electronic conductors, and the active sites for oxygen reduction reaction (ORR) are only located at the triple-phase interface. Therefore, higher operating temperatures are required to achieve a fast oxygen reduction reaction [4]. In recent decades, efforts have been focused on mixed ion-electron or even triple ($H^+/O^{2-}/e^-$) conducting cathode materials to expand cathode active sites throughout the entire cathode to improve the ORR activity.

A number of popular mixed ionic and electronic conductors (MIEC) cathodes have been developed represented by the classic $La_{0.6}Sr_{0.4}Co_{0.2}Fe_{0.8}O_{3-\delta}$ (LSCF), $Ba_{0.5}Sr_{0.5}Co_{0.8}Fe_{0.2}O_{3-\delta}$ (BSCF) and many others developed very recently, such as $SrSc_{0.175}Nb_{0.025}Co_{0.8}O_{3-\delta}$ (SSNC), $SrNb_{0.1}Co_{0.7}Fe_{0.2}O_{3-\delta}$ (SNCF), $SrCo_{0.8}Nb_{0.1}Ta_{0.1}O_{3-\delta}$ (SCNT), $PrBa_{0.5}Sr_{0.5}Co_{1.5}Fe_{0.5}O_{5+\delta}$ (PBSCF), $BaCo_{0.4}Fe_{0.4}Zr_{0.1}Y_{0.1}O_{3-\delta}$ (BCFZY)

* Corresponding authors.
** Corresponding author at: Guangdong Provincial Key Laboratory of Deep Earth Sciences and Geothermal Energy Exploitation and Utilization, Institute of Deep Earth Sciences and Green Energy, Shenzhen University, Shenzhen 518060, China.
E-mail addresses: yuanzh1216@gmail.com (Y. Zhang), meng.ni@polyu.edu.hk (M. Ni), chenbin@szu.edu.cn (B. Chen).

https://doi.org/10.1016/j.apcatb.2023.123678
Received 25 September 2023; Received in revised form 11 December 2023; Accepted 29 December 2023
Available online 2 January 2024

[5–11]. Notably, some of the above-mentioned MIEC cathodes, such as BSCF, PBSCF, and BCFZY, are found to be also triple conducting and show promising performance in proton-conducting fuel cells (PCFC) applications due to their high proton conductivity and strong hydration capabilities. There were also other attempts to enable triple conducting in cathode such as simply mixing MIEC material with the electrolyte powder to form the triple conducting cathode composite [12,13]. Self-assembly from pristine single-phase material to multiple phases is another tactful way to fabricate nanocomposites with homogeneous distribution and close contact of multiphases for optimal triple conducting [14,15]. However, the chemical instability at phase contact due to mismatched thermal expansion coefficient (TEC) or phase reaction may still be a major concern, resulting in structure failure or the formation of undesired inactive phases during long-term operation. Therefore, developing a triple conducting cathode in one single phase might be an effective solution, especially concerning the balance of long-term stability and activity issues.

The $BaCo_xFe_{(1-x)}O_{3-\delta}$ system materials exhibit excellent three-phase conductivity due to their cubic phase at > 600 °C, making them widely applied on SOFC/PCFC cathodes [16]. However, its preferred cubic structure is not stable and would change to a hexagonal phase with lower conductivity due to the lattice ion size mismatch [17]. Moreover, the presence of the alkaline earth element Ba renders $BaCo_xFe_{(1-x)}O_{3-\delta}$ insufficiently durability when exposed to acidic gases like CO_2 [18]. On the other hand, the low bond strengths of Co-O (384.5 kJ mol^{-1}) and Fe-O bond (390.4 kJ mol^{-1}) also result in higher basicity, and consequently weaker resistance to CO_2 [19], according to the Lewis acid-base theory that the reaction strength between CO_2 and metal oxides depends on the basicity of the metal oxide (i.e., its ability to provide electrons to CO_2) [18,20].

In order to improve the durability and ORR activity of $BaCo_xFe_{(1-x)}O_{3-\delta}$, the stabilization of the cubic perovskite structure is necessary. The incorporation of aliovalent Y^{3+} ions in B-site as acceptor dopants, is found to be effective in stabilizing the cubic phase and also generates oxygen vacancies by charge compensation to enhance its triple-phase conductivity [21]. For example, $BaCo_{0.7}Fe_{0.2}Y_{0.1}O_{3-\delta}$ (BCFY) exhibits triple conductivity for electrons, protons, and oxygen ions. When it is used as a cathode in SOFCs with $Sm_{0.2}Ce_{0.8}O_{1.9}$ (SDC) electrolyte, it demonstrates excellent performance (0.10 Ω cm^2 at 550 °C). Nonetheless, incorporation of Y^{3+} ions can potentially lead to the expansion of the lattice, and excessive Y^{3+} doping can also increase proton hopping distance and reduce proton conductivity [22]. In addition, Y_2O_3 may segregate in case of Ba loss or CO_2 poisoning, which is detrimental to the long-term stability [23]. The long-term stability of BCFY remains a significant challenge that needs to be addressed. On the other hand, replacing B site metal with high-valenced metals, such as Ta^{5+},and Nb^{5+} can also effectively stabilize the cubic structure, resulting in enhanced ion and electron conductivity and resistance to CO_2 [24,25]. In this study, we developed a novel single-phase perovskite cathode, $BaCo_{0.6}Fe_{0.2}Y_{0.1}Nb_{0.1}O_{3-\delta}$ (BCFYN) with fully stabilized cubic phase by Nb^{5+} doping for synergistic enhancement of activity and durability in both SOFC and PCFC. The effect of Nb doping on electrochemical performance was thoroughly investigated in terms of the lattice structure, oxygen vacancy, hydration capacity, transport kinetics, as well as durability aspects including CO_2 resistance, thermomechanical behavior. Results indicate that BCFYN is an outstanding perovskite cathode material for both SOFC and PCFC at low temperatures and Nb doping is an effective strategy for developing high-performance cathode.

2. Experimental

2.1. Powder synthesis

All $BaCo_{0.7}Fe_{0.2}Y_{0.1}O_{3-\delta}$ (BCFY) and $BaCo_{0.6}Fe_{0.2}Y_{0.1}Nb_{0.1}O_{3-\delta}$ (BCFYN) powders were synthesized using the sol-gel method. The raw materials, including $Ba(NO_3)_2$, $Co(NO_3)_2{\cdot}6\ H_2O$, $FeN_3O_9{\cdot}9\ H_2O$, $YN_3O_9{\cdot}6\ H_2O$, and $C_{10}H_5NbO_{20}{\cdot}xH_2O$ (Aladdin, analytical grade), were combined in a molar ratio of 0.05 for each synthesis process. Taking BCFYN as an example, $C_{10}H_5NbO_{20}{\cdot}xH_2O$ and citric acid (CA) were first weighed according to the stoichiometric ratio and dissolved in deionized water at 80 °C until fully dissolved. Then, $Ba(NO_3)_2$, $Co(NO_3)_2{\cdot}6\ H_2O$, $FeN_3O_9{\cdot}9\ H_2O$, and $YN_3O_9{\cdot}6\ H_2O$ were added and thoroughly dissolved at 80 °C. Subsequently, ethylenediaminetetraacetic acid (EDTA) and citric acid (CA) were added as complexing agents. The molar ratio of EDTA, CA, and total metal ions is 1:2:1. The solution's pH was controlled to be between 8 and 9 using ammonia solution. After placing the obtained gel in an oven at 180 °C for 8 h, the solid precursor was obtained. Next, different solid precursors were calcined at a fixed temperature of 1000 °C in ambient air for 5 h and then thoroughly ground to obtain the final product. The electrolytes $BaZr_{0.1}Ce_{0.7}Y_{0.1}Yb_{0.1}O_{3-\delta}$(BZCYYb) and SDC were synthesized using a similar process, with both materials calcined in ambient air for 5 h at sintering temperatures of 1000 °C and 800 °C, respectively.

2.2. Cell fabrication

SDC and BZCYYb were dry-pressed into 0.4 g substrates and sintered at 1400 °C and 1450 °C, respectively, in ambient air to form dense bases. The electrode powders were then ball-milled with isopropanol, ethylene glycol, and glycerol for 30 min to create a uniform slurry. This slurry was evenly coated on both sides of the electrolyte substrates and sintered at 800 °C for 2 h, resulting in electrolyte-supported symmetric cells. Finally, the cathode surface was uniformly brushed with silver paste at 130 °C, and silver wires were connected for current collection. The single cells with the anode (Ni+electrolyte)|electrolyte|cathode configuration were prepared using the dry-pressed co-sintering method. For example, NiO, BZCYYb, and soluble starch (in *a* mass ratio of 6:4:1) were thoroughly mixed and first pressed to form an anode-supported body. Then, BZCYYb was uniformly coated on the anode's surface, and both powders were co-pressed to create a two-layered substrate. Afterward, the substrate was sintered at 1450 °C in ambient air for 5 h (for SDC electrolyte cells, sintering was at 1400 °C for 5 h). Finally, the cathode slurry was spray-coated on the center surface (circular area of 0.45 cm^2), and the complete single cell was obtained after sintering at 800 °C in ambient air for 2 h.

2.3. Characterizations and electrochemical measurement

Using a high-temperature heating furnace from KJ Group, the symmetric cells were heated from room temperature to 700 °C over 70 min. Electrochemical impedance spectroscopy (EIS) measurements were performed on the Princeton Electrochemical Workstation in the frequency range of 100 kHz to 0.1 Hz at 30 mV open circuit potential. Starting at 700 °C, the EIS measurements were taken with a 50 °C decrement until 450 °C. The EIS data were then fitted with equivalent circuit models using Zview software. I-V and I-P polarization curves were collected using a Keithley 2460 measurement instrument. During the experiments, dry hydrogen gas was supplied to the anode side at a flow rate of 80 ml min^{-1}, while the cathode side was exposed to ambient air.

2.4. Characterisation

Crystal structure of BCFYN and BCFY were determined by X-ray diffraction (XRD, Bruker D8 Advance, Germany). The fine details of the BCFYN and BCFY microstructures were explored using high-resolution transmission electron microscopy (HR-TEM) with the FEI Talos F200x instrument. Additionally, we acquired element distribution information through energy-dispersive X-ray (EDX) mappings. To examine the oxidation state of elements in BCFYN and BCFY, we performed X-ray photoelectron spectroscopy (XPS) analysis using the PHI 5000 Versaprobe III instrument at ambient temperature. The thermogravimetric

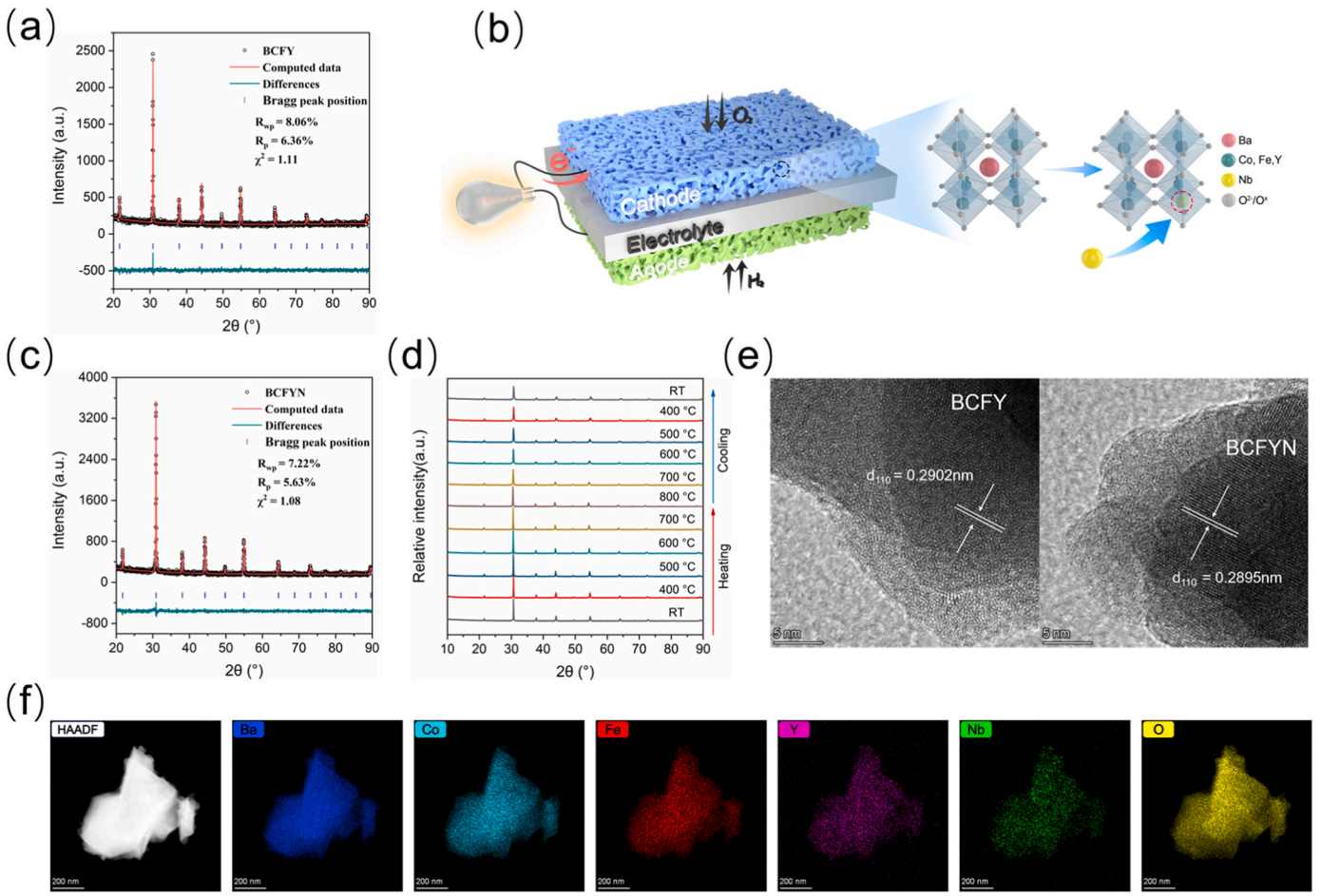

Fig. 1. (a) Rietveld refinement profiles of the BCFY sample. (b) Schematic diagram of the Nb substitution in ABO_3-type perovskite structure. (c) Rietveld refinement profiles of the BCFYN sample. (d) HT-XRD patterns of BCFYN powder. (e) HR-TEM image of BCFY and BCFYN. (f) EDX-mapping result of BCFYN.

characteristics of the samples were determined using a TGA system (PerkinElmer STA 8000). When using TGA to estimating proton concentration, the sample was heated from room temperature to 800 °C in dry air, with a heating rate of 5 °C min^{-1}. Subsequently, the TG analyzer recorded weight data during the cooling stage (5 °C min^{-1}) from 800 °C to 200 °C under both dry and wet air, respectively. To assess the ability of the samples to release oxygen, we conducted oxygen temperature-programmed desorption (O_2-TPD) using a mass spectrometer (Hiden Analytica, HPR20). The ECR test involved rapidly altering the oxygen partial pressure from 0.21 to 0.1 atm. Specifically, measurements for ECR between 500 and 650 °C were performed using a Keithley 2460 source meter. The thermal expansion coefficient (TEC) was obtained in the air using a Netzsch DIL 402 C/3/G dilatometer ranging from 200–800 °C.

3. Results and discussion

Fig. 1a-c, and Fig. S1 shows the X-ray diffraction (XRD) patterns of BCFY and BCFYN and the corresponding refinement results, all of which exhibit a pure cubic perovskite phase (Pm-3 m) at room temperature, confirming the successful Nb substitution in the B-site of elements with no segregation as schemed in Fig. 1b, corresponding SEM diagrams shown in Fig. S2. The lattice parameters for BCFYN were refined to be a=b=c= 4.0945 Å (Rp=5.63%, Rwp=7.22%, χ^2 =1.08), while a=b=c= 4.1035 Å (Rp=6.36%, Rwp=8.06%, χ^2 =1.11) for BCFY, slightly larger than BCFYN. This also confirms the successful Nb substitution in the BCFY lattice due to the contraction in the unit cell volume caused by the smaller ionic radius of Nb^{5+} compared to $Co^{3+/4+}$. To assess the lattice evolution of the Nb-doped BCFYN at working conditions, high-temperature X-ray diffraction (HT-XRD) analysis was performed in air from room temperature up to 800 °C (Fig. 1d). The results show that the BCFYN sample maintains its cubic structure at all tested temperatures. HR-TEM measurements (Fig. 1e) confirm the d-spacings of 0.2895(110) and 0.2902(110) for BCFYN and BCFY, respectively, in agreement with the XRD refinement results. Fig. 1f shows the EDX mapping analysis of BCFYN perovskite, again indicating uniform Nb distribution within the lattice. The point EDX results for BCFYN (Fig. S3) also match well with the designed stoichiometric ratio of elements. The corresponding EDX mapping for BCFY is provided in Fig. S4. Ensuring good chemical compatibility between cathode and electrolyte is a crucial factor for long-term stable operation even at intermediate temperatures. Considering that the cathode layer is prepared at 800 °C for 2 h, which is quite high for the potential formation of the insulating phase. Therefore, the phase reactivity between BCFYN and BZCYYb (or SDC) was examined. BCFYN and electrolyte powder were mixed in a 1:1 mass ratio and calcined at 800 °C for 2 h. No peaks of the reacted products were observed between BCFYN and BZCYYb, as well as SDC as shown in Fig. S5, indicating excellent chemical compatibility between BCFYN and both SDC and BZCYYb electrolytes.

The ORR activity of perovskite cathode materials was evaluated through EIS tests of symmetric cells using SDC or BZCYYb as the electrolyte, i.e. BCFYN|SDC|BCFYN and BCFYN|BZCYYb|BCFYN, in the temperature range from 450 to 700 °C in air. Fig. 2a shows the Arrhenius plot of the area-specific resistance (ASR) deduced from EIS of symmetric cells with SDC electrolyte. At 500 °C, the ASR values for BCFY and BCFYN are 0.94 and 0.38 Ω cm^2, respectively. This indicates

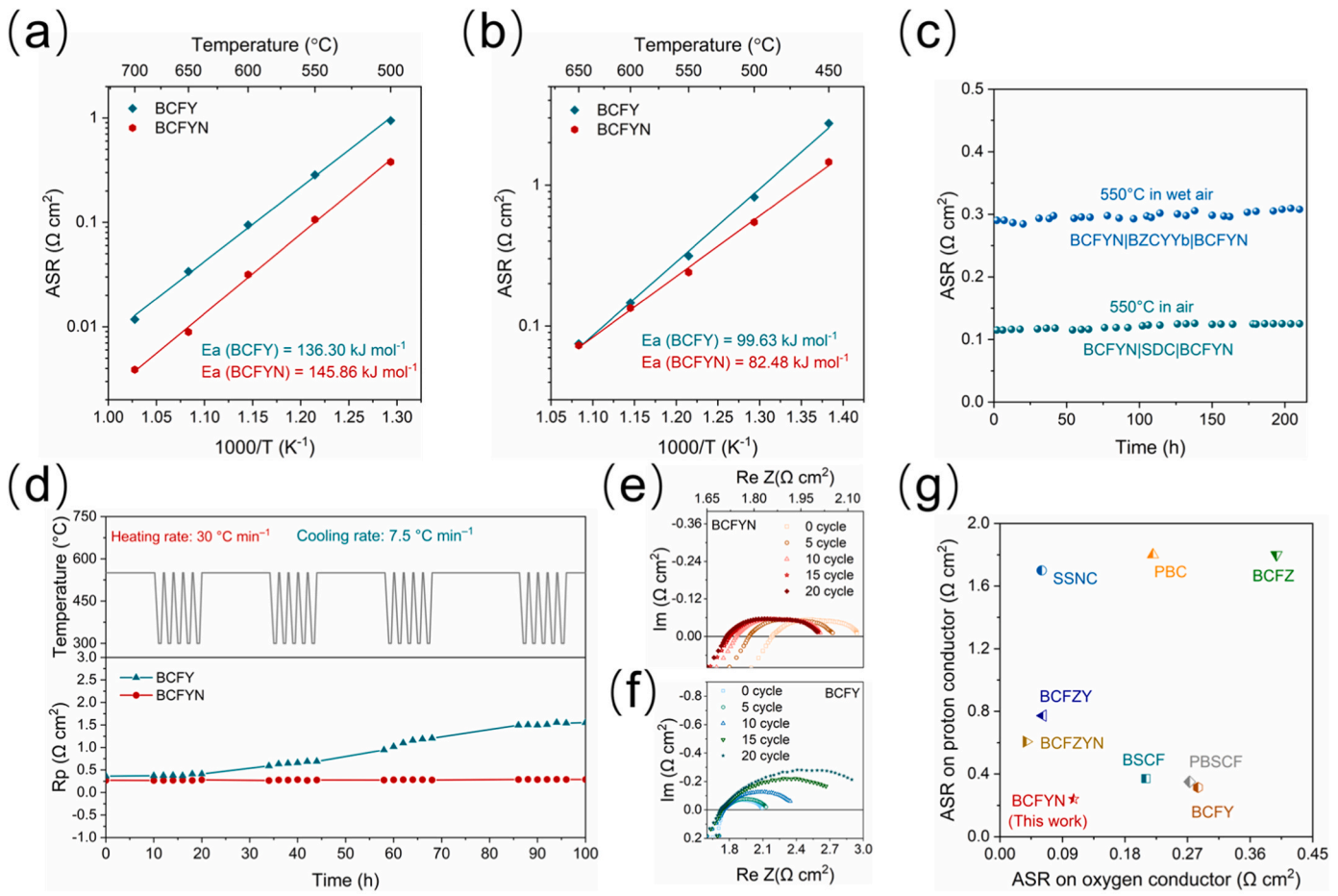

Fig. 2. (a) ASRs of SDC-supported symmetrical cells with BCFY and BCFYN cathodes between 500 and 700 °C in dry air. (b) ASRs of BZCYYb-supported symmetrical cells with BCFY and BCFYN cathodes between 450 and 650 °C in wet air (3 vol%). (c) 200-hours stability of BCFYN on symmetric cells both in air and in wet air (3 vol%). (d) The ASR response of BCFY and BCFYN-based symmetric cell electrodes during 20 rapid thermal cycles between 550 °C and 300 °C. Representative EIS Nyquist plots for the (e) BCFYN and (f) BCFY symmetric cell after cycling in BZCYYb. (g) Comparison of ASRs of BCFY, BCFYN, and classic cathodes at 550 °C.

that Nb doping at the B-site of perovskite enhances the ORR activity in oxygen ion-conducing fuel cells. Fig. 2b shows the ASR of symmetric cells based on the proton-conducting BZCYYb electrolyte using BCFY and BCFYN as electrodes in 3 vol% H_2O-air condition. At 500 °C, the ASR values for BCFY and BCFYN are 0.82 and 0.54 Ω cm^2, respectively. These results align with those observed with SDC electrolyte, demonstrating the positive effect of Nb doping at the B-site of perovskite on ORR. Notably, the BCFYN exhibits lower activation energy (~82.48 kJ mol^{-1}) *v.s.* BCFY(~99.63 kJ mol^{-1}), making BCFYN cathode a promising candidate for intermediate to low-temperature PCFC applications, e.g. an outstanding low ASR of 1.45 Ω cm^2 when even further extended to 450 °C. The stability of BCFYN was investigated through a 200-hour EIS test of symmetric cells at 550 °C. Results in Fig. 2c revealed that the BCFYN electrode in dry air exhibited stable performance with ASR around 0.115–0.125 Ω cm^2 on SDC electrolyte, showing no significant degradation. Similarly, on the BZCYYb electrolyte in weted air (3 vol%) at 550 °C, the BCFYN electrode also maintained its ASR at approximately 0.30 Ω cm^2 throughout the 200-hour test, indicating excellent electrochemical stability.

To assess the BCFY and BCFYN electrode's thermal cycling stability, rigorous thermal cycling was performed on symmetric cells at the operational temperature with a fast heating rate of 30 °C min^{-1} and passive cooling at about 7.5 °C min^{-1}, shown in Fig. 2d and Fig. S6. After 20 rapid temperature cycles within 100 h, the BCFYN electrode on SDC substrate maintained a constant ASR value of 0.032 Ω cm^2. On BZCYYb substrate, the ASR of BCFYN also remained stable, slightly increasing from 0.27 to 0.285 Ω cm^2, while the ASR of BCFY increased dramatically from 0.36 to 1.54 Ω cm^2. The comparison of EIS results during thermal cycling is shown in Fig. 2e and f and Fig. S6 confirms the excellent durability and good compatibility of the BCFYN on SDC and BZCYYb electrolytes, as evidenced by the stable overpotential resistance (R_p) and ohmic resistance (R_{ohmic}). SEM images in Fig. S7 also revealed the good compatibility between the BCFYN electrode and electrolyte with no delaminations/cracks observed. To the best knowledge of the authors, the BCFYN outperforms most classical cathodes (Fig. 2g, details given in Tables S1 and S2), especially in the realm of intermediate-temperature PCFCs.

To explain the enhancement mechanism of Nb doping on ORR activity, we employed the distribution of relaxation time (DRT) technique to interpret the impedance response of BCFY and BCFYN, thereby identifying the rate-determining steps in the ORR process. DRT plots of electrodes on SDC (Fig. 3a) and BZCYYb (Fig. 3b) electrolytes in air at 550 °C both exhibit three distinct peaks, denoted as high-frequency (HF), intermediate-frequency (IF) and low-frequency (LF) peaks corresponding to three processes: transfer of ions from the electrolyte to the electrode at the three-phase boundary; ion migration or surface exchange within the electrode bulk; and gas diffusion, respectively [24,26,27]. BCFYN exhibits noticeable impedance reduction in the intermediate-frequency (IF) range compared to BCFY on SDC electrolyte, indicating significant enhancement of surface oxygen exchange kinetics due to Nb doping. In the case of BZCYYb electrolyte, the BCFYN also demonstrates lower impedance in the IF regions than BCFY. In particular, the HF peak of BCFYN is also reduced compared to BCFY. This signifies the synergic enhancement of surface oxygen exchange and

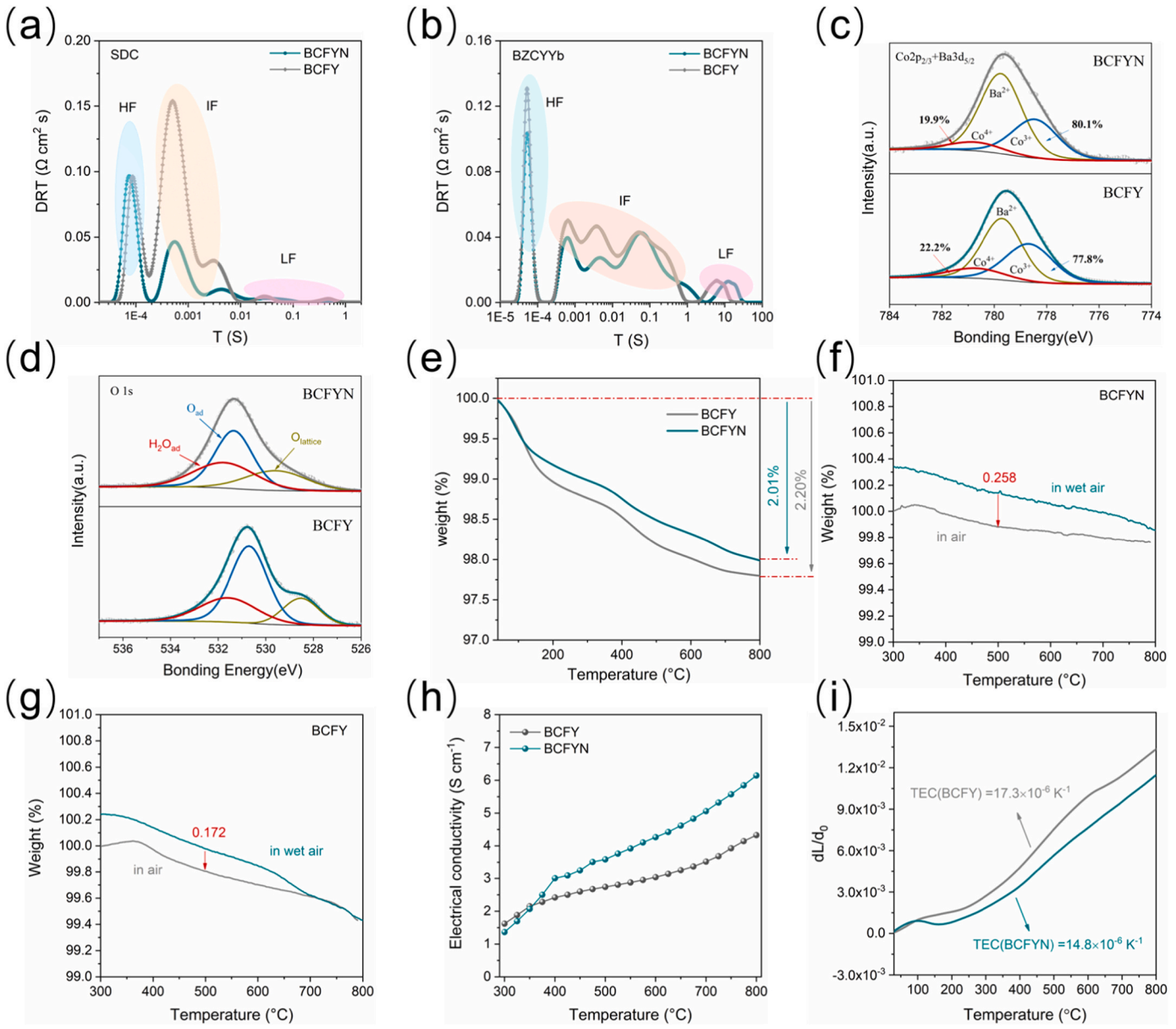

Fig. 3. DRT of BCFYN and BCFY electrodes at 550 °C on (a) SDC and (b) BZCYYb electrolyte. XPS spectra of BCFY and BCFYN powders: (c) Co 2p and (d) O 1 s (e) The TGA curves of BCFY and BCFYN from RT to 800 °C. The TGA of (f) BCFYN and (g) BCFY during the cooling stage under dry and wet air. (h) The electrical conductivity of BCFY and BCFYN. (i) Thermal-expansion curves of dense BCFY and BCFYN bar specimens from 25 to 800 °C in air.

charge transfer by Nb doping, leading to its superior performance at low temperatures on the BZCYYb electrolyte as shown in Fig. 2b [28]. Considering the charge transfer process (i.e. oxygen ion transfer at TPB) in SDC-based symmetrical cells was not rate-determining and did not show reduction after Nb doping, we can attribute the improved charge transfer in BZCYYb-based cells to the facilitated proton transfer process by Nb doping.

The ORR kinetics and charge transfer largely depend on the oxidation state of transition metals at the B-site of perovskite and the concentration of oxygen vacancies [29]. X-ray photoelectron spectroscopy (XPS) was therefore utilized to probe the oxidation states of elements in BCFYN perovskite. The Co $2p_{3/2}$ and O 1 s spectra of BCFY and BCFYN samples are presented in Fig. 3c and d, respectively. The binding energies of Co^{3+} and Co^{4+} were referred to be 778.6 ± 0.3 eV and 780.7 ± 0.3 eV, respectively in the literature [30]. Similarly, the binding energy (BE) of Co^{3+} is also observed at 778.45 eV in BCFYN, which is pronouncedly lower than the 778.67 eV for BCFY. The lowered binding energies of metal ions usually imply the enhanced oxygen migration rates within the oxide bulk and accelerated oxygen exchange kinetics on the oxide surface [31]. Moreover, from the O 1 s XPS results in Fig. 3d, the binding energies for lattice oxygen ($O_{lattice}$) in BCFY and BCFYN are 528.5 eV and 529.6 eV, respectively. The higher BE of $O_{lattice}$ implies weaker Coulombic forces between B-site ions and $O_{lattice}$ in BCFYN, as evidence of enhanced lattice oxygen mobility [32], which is beneficial to the BCFYN electrode's ORR activity. Besides, the higher ratio of lattice oxygen to adsorb oxygen ($O_{lattice}/O_{ad}$) is observed in BCFYN (~0.50) as compared to that of BCFY (~0.32), which indicates the reduced oxygen vacancy caused by the charge compensation to high-valenced Nb^{5+} doping. As argued in a previous work [33], the excessive oxygen vacancies may cause over-competition of water adsorption that is negative for ORR activity. Therefore, we conjure that the enhanced ORR is due to the optimized oxygen vacancies (i. e. reduced in this BCFY system by Nb doping), which are seemingly conflicting with the traditional positive correlation between oxygen vacancy and ORR activity. Studies also have

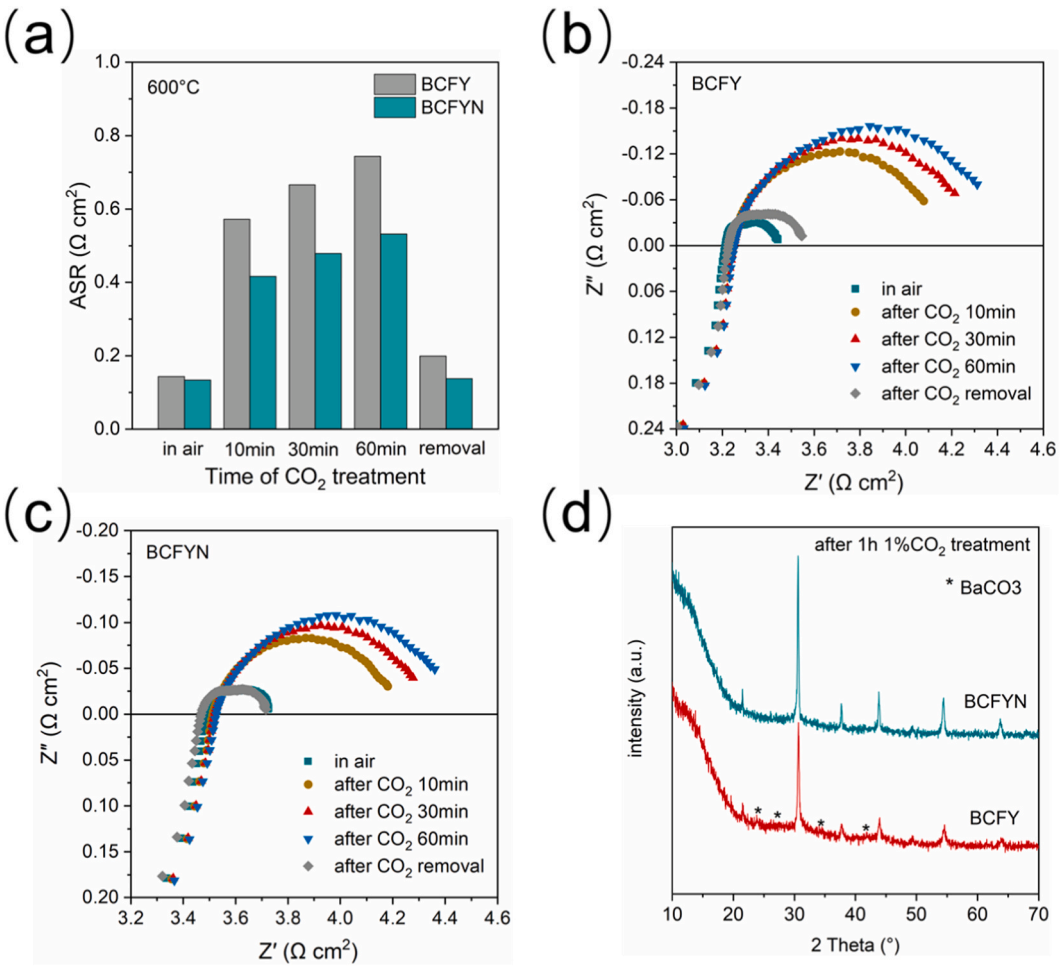

Fig. 4. (a) The ASR of BCFY and BCFYN cathodes after exposure to 1% CO_2 in wet air at 600 °C. The "removal" indicates the ASRs of cathodes after removing the CO_2 from air for 30 min. Electrochemical impedance spectra (EIS) of (b) BCFY and (c) BCFYN cathodes measured in the presence of CO_2 at 600 °C. (d) XRD results after 1-hour treatment of BCFY and BCFYN in 1% CO_2 concentration air.

revealed that proton conduction does not simply depend on the concentration of oxygen vacancies [34–37]. In effect, excessive oxygen vacancies (correspondingly, lower surface exposed $O_{lattice}$) may even hinder the proton transport through the Grotthuss mechanism due to the lowered hydroxide defects ($OH_o^{\cdot}$) conce ntration by the competition oxygen absorption reaction to the hydration reaction.

To support this argument, the weight loss curves in dry air and wet air are measured from room temperature (RT) to 800 °C in Fig. 3e-g. The TGA curves in Fig. 3e illustrate the weight loss of BCFY and BCFYN in the dry air environment from room temperature (RT) to 800 °C. Below 130 °C, the quick weight loss is due to the desorption of surface-adsorbed water, while the continuous weight decrease from 130 to 800 °C was caused by the loss of hydrated lattice water and the generation of oxygen vacancy, corresponding to the breaking of Co-O bonds and subsequent oxygen release from the crystal lattice [38]. Till 800 °C, BCFY and BCFYN samples show weight losses of 2.20% and 2.01%, respectively. To individually measure the mass loss due to desorption of hydrated water, we also compare the TGA curves in wet air and dry air when cooling from 800 °C to 300 °C (Fig. 3f and g). In dry air, we can attribute the mass increase during cooling to oxygen uptake to fill the vacancy, while in wet air, both oxygen and H_2O uptake contribute to the increase [39]. The value difference of mass change in dry and wet air is merely due to the water uptake, representing the hydration capacity of the material. Therefore, it can be concluded that BCFYN has better hydration capability (e. g. 0.258% water uptake in BCFYN v.s. 0.172% in BCFY at 500 °C). Considering that the total mass loss of BCFYN up heating is less(2.01%) compared to that of BCFY(2.20%), while its water desorption is higher, we can confirm that the oxygen vacancies are indeed significantly reduced by Nb doping, inconsistent with the O 1 s peaks from XPS and other works on high valenced Nb doping perovskites [40–42].

To investigate the effect of Nb doping on the oxygen desorption behavior, O_2-TPD experiments were conducted in flowing argon. Fig. S8 shows the O_2-TPD curves of BCFY and BCFYN samples captured by the thermal conductivity detector (TCD) signal. The lower onset temperatures(~ 310 °C) for lattice oxygen desorption in BCFYN than BCFY(~ 440 °C) indicate faster surface oxygen exchange and oxygen ion migration within the perovskite structure [43], confirming that the presence of slight Nb at the B site facilitates oxygen migration, which is consistent with XPS results.

Subsequently, the ECR method was used to study how oxygen ions move through BCFY and BCFYN and how the surfaces of these materials interact. To make it easy to compare, Fig. S9 shows graphs of the ECR responses of BCFY and BCFYN at 550 °C. In this figure, we provide values for the diffusion coefficient (D_{chem}) and surface exchange constant (k_{chem}) for both samples. These values were obtained using the ECR method and cover temperatures from 500 to 650 °C. As depicted in Fig. S9, the D_{chem} and k_{chem} values of BCFYN surpass those of BCFY. This suggests that the slight introduction of Nb at the B-site has significantly enhanced both the oxygen surface exchange and bulk diffusion in BCFYN, thereby improving its ORR activity.

The overall conductivity of the cathode is another key factor

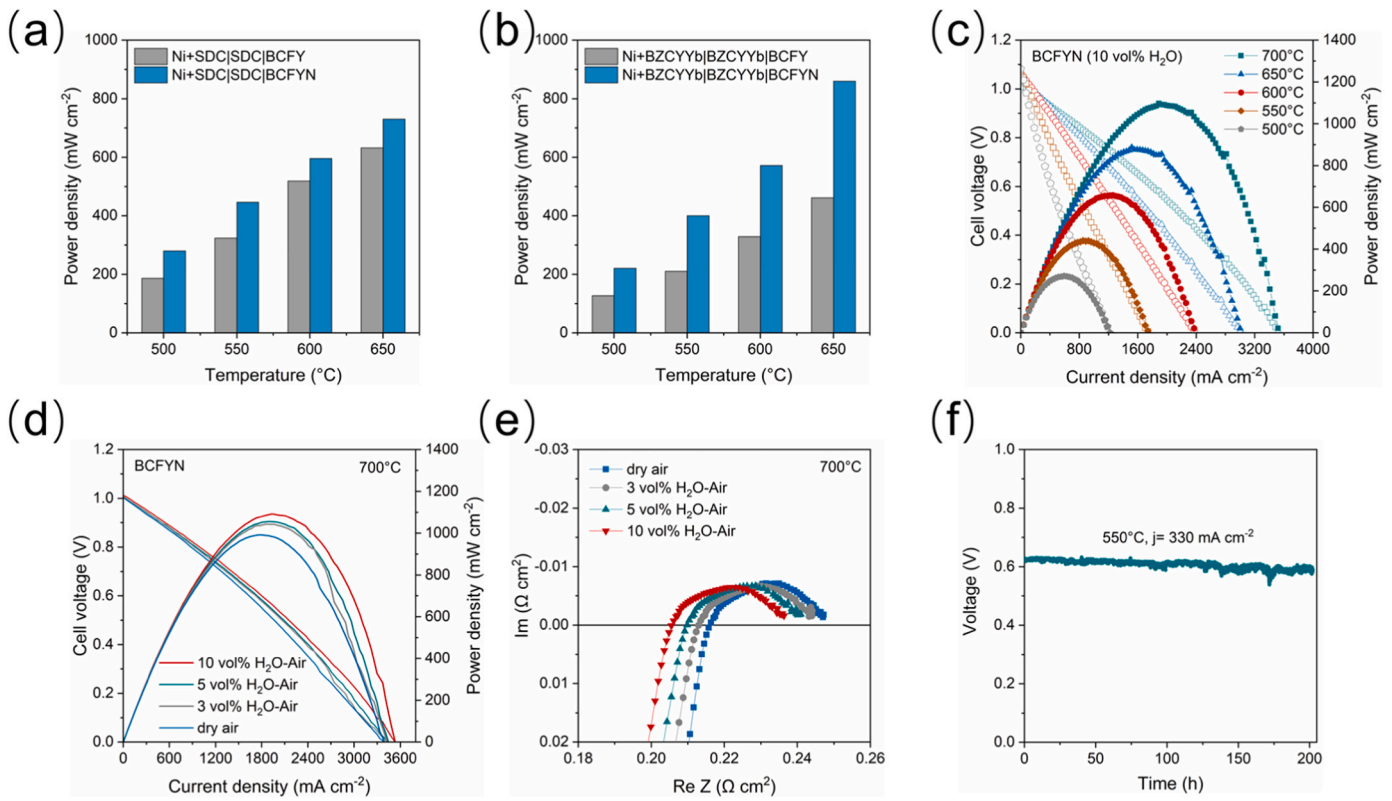

Fig. 5. The peak power density of BCFY and BCFYN on single cells with (a) SDC electrolyte and (b) BZCYYb electrolyte in ambient air from 500–650 °C. (c) I-V and I-P curves of Ni+BZCYYb|BZCYYb|BCFYN in 10 vol% H_2O-air conditions. (d) I-V and I-P curves of Ni+BZCYYb|BZCYYb|BCFYN in wetted air, corresponding EIS given in (e). (f) BCFYN single cell at 330 mA cm^{-2} at 550 °C for 200 h.

governing the ORR activity. As depicted in Fig. 3h, BCFYN demonstrates enhanced electronic conductivity to BCFY within the operating temperature range, i.e. reaching a maximum value of 6 S cm^{-1} at 650 °C. The electronic conductivity of cubic perovskite is mainly correlated to the hole jumping process and excessive generation of oxygen vacancy could annihilate the concentration of holes and thus impede the hole jumping on the Fe(Co)-O-Fe(Co) bond [39,44]. Here in the p-type conducting material of BCFY, the enhancement of electronic conductivity after 400 °C also implies that the generation of oxygen vacancies is suppressed by Nb doping observed.

In order to achieve long-term stability of fuel cell electrodes at elevated temperatures, it is essential to maintain compatible thermal-mechanical properties between the adjoined cell components. Usually, a significant mismatch of thermal expansion coefficient (TECs) exists in the porous cathode and electrolyte, resulting in interface delamination [45]. Under ambient air conditions, the TEC curves of BCFY and BCFYN were determined as shown in Fig. 3i. BCFYN exhibited a slightly lower average TEC (14.8 $\times 10^{-6}$ K^{-1}) compared to BCFY (17.3 $\times 10^{-6}$ K^{-1}) in the range of 25–800 °C, suggesting that the introduction of a small amount of Nb at the B-site, replacing Co, can effectively mitigate the TEC of the perovskite structure and improve the durability as showcased in thermal cycle test of Fig. 2d.

In addition to TEC mismatch, CO_2 poisoning is another key bottlenecking factor to the durability of the cathode especially in proton-conducting fuel cells. Even the presence of trace CO_2 in the air (~3 ppm) can lead to structural degradation of the electrode since the alkaline metal Ba and Sr in most perovskite cathodes are thermodynamically prone to reacting with CO_2, forming carbonates on the surface, which hinders surface oxygen exchange and adversely affects ORR activity, cell performance, and long-term stability [46,47]. Therefore, we measured the ASR values of electrodes on BZCYYb-based symmetrical cells under wet air with 1%vol CO_2 at 600 °C as summarized in Fig. 4a with the corresponding EIS data presented in Fig. 4b and c. The BCFYN shows a smaller ASR compared to BCFY during the 60-minute CO_2 poisoning, highlighting its stronger CO_2 resistance. After the CO_2 treatment, the gas is switched back to CO_2-free wet air for 30 min, and the ASR of BCFYN is fully recovered to ~ 0.138 Ω cm^2, very close to its initial value, whereas BCFY's ASR remains about 40% higher, underscoring BCFYN's enhanced CO_2 resistance and excellent recoverability due to Nb doping. This is attributed to the relatively higher acidity of Nb^{5+} than Co according to the Lewis acid-base theory [7]. To clarify, the O 1 s BE of BCFYN can be used as a descriptor for the basicity of metal oxide [19]. We can clearly see a 1.1 eV shift towards higher energy after Nb doping (Fig. 3d), which suggests that BCFYN has a reduced electron-donating capability and higher acidity, resulting in its enhanced resistance to CO_2. To further validate the improved resistance of BCFYN to CO_2, we conducted the XRD analysis of both samples after exposure to 1% CO_2 at 600 °C for 1 h. From Fig. 4d, it can be observed that distinct diffraction peaks corresponding to Barium carbonate (JCPDF#05-0378) are present in BCFY, whereas they are absent in the sample of BCFYN. This does prove that BCFYN exhibits stronger resistance to CO_2 due to the higher acidity of Nb^{5+} than $Co^{3+/4+}$, $Fe^{2+/3+}$doping [48].

To showcase the good electrochemical performance of BCFYN in the full cells, we fabricated anode-supported fuel cells configured as Ni+SDC|SDC|BCFYN (BCFY) and Ni+BZCYYb|BZCYYb|BCFYN (BCFY). The cross-sectional SEM images of the single cells after reduction with BCFYN cathodes are shown in Fig. S10 with about 20–30 μm electrolyte. The images reveal that the cathode and electrolyte are tightly bonded after the reduction, with no observable delamination or fracture. At temperatures ranging from 500 °C to 650 °C, single cells with BCFYN demonstrated significantly enhanced performance than the cells with BCFY in ambient air, regardless of operating in PCFC or SOFC, as depicted in Fig. 5a and b. For example, at 650 °C, the single cell using

SDC electrolyte demonstrates a maximum power density (PPD) of 730 mW cm^{-2}, while the single cell using BZCYYb electrolyte exhibits a PPD of 860 mW cm^{-2}. The corresponding impedance curves and I-V curves are presented in Figs. S11-S13.

As already stated, the ORR activity of cathode material is highly correlated to the hydration capacity, therefore the sufficient supply of water from air can be a key operating parameter to the actual ORR performance of cathode materials in proton conducting fuel cells [49]. We investigated the impact of varying water content on the peak power density and impedance of the BCFYN. Fig. 5c presents the maximum power density of the BCFYN cathode in single cells under 10 vol% H_2O-air from 700 °C to 500 °C, as a comparison to the dry air condition in Fig. S11. At 700 °C, BCFYN achieves a 10% enhancement (1100 mW cm^{-2} in wet air v.s. 990 mW cm^{-2} in dry air). Besides, we tested the single cell performance with BCFYN cathode at different levels of water content in the air (0/3/5/10 vol% H_2O-air) at 700 °C in Fig. 5d and e. It's evident that increasing air humidity is beneficial to the cathode activity and the peak power density (PPD). The enhanced PPD and significantly reduced ohmic resistance (Fig. 5e) under higher water content again verified that hydration is key to the proton transportation process [5,50,51]. On this basis, the Nb doping effectively promotes the proton transportation as seen from the reduced ohmic resistance that is caused by the improved hydration capacity (Fig. S11). Moreover, the BCFYN single cell demonstrates remarkable durability for more than 200 h, at a current density of 330 mA cm^{-2} at 550 °C as depicted in Fig. 5f.

4. Conclusions

In summary, our work has led to the successful development of a high-performance PCFC/SOFC cathode material—BCFYN, through niobium doping at the B-site cation of the perovskite lattice. The superior ASR values of BCFYN are only 0.37 Ω cm^2 and 0.54 Ω cm^2, respectively, at 500 °C when used in symmetric cells with SDC and BZCYYb electrolytes. Additionally, BCFYN exhibits remarkable stability, showing no significant performance degradation during 200 h of operation and no noticeable changes after 20 rapid temperature cycling tests within 100 h. Characterizations reveal that Nb doping optimizes the surface oxygen exchange kinetics and proton transfer process through enhanced hydration capacity and optimized oxygen vacancy, in addition, the improved CO_2 resistance and reduced TEC facilitate the durability of the cathode. These findings underscore the significant potential of BCFYN as a prospective candidate for cathodes in SOFC/PCFC applications.

CRediT authorship contribution statement

Zhang Yuan: Conceptualization, Supervision, Writing – original draft, Writing – review & editing. **Li Junbiao:** Data curation, Software. **You Junda:** Data curation, Software. **Yang Hongxin:** Data curation. **Zhu Haojie:** Data curation. **Ni Meng:** Conceptualization, Supervision, Writing – original draft. **Shao Zongping:** Supervision. **Chen Bin:** Conceptualization, Writing – original draft, Writing – review & editing. **Liu Zhipeng:** Data curation, Investigation, Visualization, Writing – original draft. **Xie Heping:** Funding acquisition, Supervision.

Declaration of Competing Interest

The authors declare that they have no known competing financial interests or personal relationships that could have appeared to influence the work reported in this paper.

Data availability

Data will be made available on request.

Acknowledgement

This work was supported by the National Natural Science Foundation of China Project (grant numbers 51827901, 52006150, and 22109101). We also extend our thanks to the Program for Guang Dong Introducing Innovative and Entrepreneurial Teams (Grant No. 2019ZT08G315), the fellowship of China Postdoctoral Science Foundation (No. 2021T140471) and Guangdong Basic and Applied Basic Research Foundation (2023A1515011205) and Shenzhen Science and Technology Program (Grant No. RCBS20210609103648039 and No. JCYJ20210324093008021) for their support.

Appendix A. Supporting information

Supplementary data associated with this article can be found in the online version at doi:10.1016/j.apcatb.2023.123678.

References

[1] Y. Zhang, R. Knibbe, J. Sunarso, Y. Zhong, W. Zhou, Z. Shao, Z. Zhu, Recent progress on advanced materials for solid-oxide fuel cells operating below 500 °C, Adv. Mater. 29 (2017) 1700132, https://doi.org/10.1002/adma.201700132.
[2] E.D. Wachsman, K.T. Lee, Lowering the temperature of solid oxide fuel cells, Science 334 (2011) 935–939, https://doi.org/10.1126/science.1204090.
[3] Y. Gao, M. Zhang, M. Fu, W. Hu, H. Tong, Z. Tao, A comprehensive review of recent progresses in cathode materials for Proton-conducting SOFCs, Energy Rev. 2 (2023) 100038, https://doi.org/10.1016/j.enrev.2023.100038.
[4] J. Nielsen, J. Hjelm, Impedance of SOFC electrodes: a review and a comprehensive case study on the impedance of LSM:YSZ cathodes, Electrochim. Acta 115 (2014) 31–45, https://doi.org/10.1016/j.electacta.2013.10.053.
[5] S. Choi, C.J. Kucharczyk, Y. Liang, X. Zhang, I. Takeuchi, H.-I. Ji, S.M. Haile, Exceptional power density and stability at intermediate temperatures in protonic ceramic fuel cells, Nat. Energy 3 (2018) 202–210, https://doi.org/10.1038/s41560-017-0085-9.
[6] M. Li, M. Zhao, F. Li, W. Zhou, V.K. Peterson, X. Xu, Z. Shao, I. Gentle, Z. Zhu, A niobium and tantalum co-doped perovskite cathode for solid oxide fuel cells operating below 500 °C, Nat. Commun. 8 (2017) 13990, https://doi.org/10.1038/ncomms13990.
[7] Y. Zhang, G. Yang, G. Chen, R. Ran, W. Zhou, Z. Shao, Evaluation of the CO_2 poisoning effect on a highly active cathode $SrSc_{0.175}Nb_{0.025}Co_{0.8}O_{3-\delta}$ in the oxygen reduction reaction, ACS Appl. Mater. Interfaces 8 (2016) 3003–3011, https://doi.org/10.1021/acsami.5b09780.
[8] Y. Zhu, W. Zhou, Z.-G. Chen, Y. Chen, C. Su, M.O. Tadé, Z. Shao, $SrNb_{0.1}Co_{0.7}Fe_{0.2}O_{3-\delta}$ perovskite as a next-generation electrocatalyst for oxygen evolution in alkaline solution, Angew. Chem. Int. Ed. 54 (2015) 3897–3901, https://doi.org/10.1002/anie.201408998.
[9] C. Duan, J. Tong, M. Shang, S. Nikodemski, M. Sanders, S. Ricote, A. Almansoori, R. O'Hayre, Readily processed protonic ceramic fuel cells with high performance at low temperatures, Science 349 (2015) 1321–1326, https://doi.org/10.1126/science.aab3987.
[10] Z. Shao, S.M. Haile, A high-performance cathode for the next generation of solid-oxide fuel cells, Nature 431 (2004) 170–173, https://doi.org/10.1038/nature02863.
[11] J.A. Lane, S.J. Benson, D. Waller, Oxygen transport in $La_{0.6}Sr_{0.4}Co_{0.2}Fe_{0.8}O_{3-\delta}$, Solid State Ion. 121 (1999) 201–208, https://doi.org/10.1016/S0167-2738(99)00014-4.
[12] T. Matsui, K. Manriki, K. Miyazaki, H. Muroyama, K. Eguchi, A new oxygen reduction electrocatalyst of barium lanthanide cobaltate for composite cathodes of proton-conducting ceramic fuel cells, J. Mater. Chem. A 6 (2018) 14188–14194, https://doi.org/10.1039/C8TA04093A.
[13] R. Peng, T. Wu, W. Liu, X. Liu, G. Meng, Cathode processes and materials for solid oxide fuel cells with proton conductors as electrolytes, J. Mater. Chem. 20 (2010) 6218, https://doi.org/10.1039/c0jm00350f.
[14] Z. Zhao, M. Zou, H. Huang, X. Zhai, H. Wofford, J. Tong, Insight of $BaCe_{0.5}Fe_{0.5}O_{3-\delta}$ twin perovskite oxide composite for solid oxide electrochemical cells, J. Am. Ceram. Soc. 106 (2023) 186–200, https://doi.org/10.1111/jace.18643.
[15] Y. Song, Y. Chen, W. Wang, C. Zhou, Y. Zhong, G. Yang, W. Zhou, M. Liu, Z. Shao, Self-assembled triple-conducting nanocomposite as a superior protonic ceramic fuel cell cathode, Joule 3 (2019) 2842–2853, https://doi.org/10.1016/j.joule.2019.07.004.
[16] Y. Yin, Y. Zhou, Y. Gu, L. Bi, Successful preparation of $BaCo_{0.5}Fe_{0.5}O_{3-\delta}$ cathode oxide by rapidly cooling allowing for high-performance proton-conducting solid oxide fuel cells, J. Adv. Ceram. 12 (2023) 587–597, https://doi.org/10.26599/JAC.2023.9220707.
[17] H. Kruidhof, H.J.M. Bouwmeester, R.H.E. v Doorn, A.J. Burggraaf, Influence of order-disorder transitions on oxygen permeability through selected nonstoichiometric perovskite-type oxides, Solid State Ion. 63 (1993) 816–822, https://doi.org/10.1016/0167-2738(93)90202-E.

[18] Y. Zhu, J. Sunarso, W. Zhou, Z. Shao, Probing CO_2 reaction mechanisms and effects on the $SrNb_{0.1}Co_{0.9-x}Fe_xO_{3-\delta}$ cathodes for solid oxide fuel cells, Appl. Catal. B Environ. 172–173 (2015) 52–57, https://doi.org/10.1016/j.apcatb.2015.02.010.

[19] W. Chen, C. Chen, L. Winnubst, Ta-doped $SrCo_{0.8}Fe_{0.2}O_{3-\delta}$ membranes: phase stability and oxygen permeation in CO_2 atmosphere, Solid State Ion. 196 (2011) 30–33, https://doi.org/10.1016/j.ssi.2011.06.011.

[20] W. Chen, C. Chen, H.J.M. Bouwmeester, A. Nijmeijer, L. Winnubst, Oxygen-selective membranes integrated with oxy-fuel combustion, J. Memb. Sci. 463 (2014) 166–172, https://doi.org/10.1016/j.memsci.2014.03.063.

[21] W. He, X. Wu, G. Yang, H. Shi, F. Dong, M. Ni, $BaCo_{0.7}Fe_{0.22}Y_{0.08}O_{3-\delta}$ as an active oxygen reduction electrocatalyst for low-temperature solid oxide fuel cells below 600 °C, ACS Energy Lett. 2 (2017) 301–305, https://doi.org/10.1021/acsenergylett.6b00617.

[22] R.D. Shannon, Revised effective ionic radii and systematic studies of interatomic distances in halides and chalcogenides, Acta Crystallogr. Sect. A. 32 (1976) 751–767, https://doi.org/10.1107/S0567739476001551.

[23] J.H. Duffy, H.W. Abernathy, K.S. Brinkman, Tuning proton kinetics in $BaCo_{0.4}Fe_{0.4}Zr_{0.2-X}Y_XO_{3-\delta}$ triple ionic-electronic conductors via aliovalent substitution, J. Mater. Chem. A 11 (2023) 8929–8938, https://doi.org/10.1039/D3TA00654A.

[24] J.H. Kim, D. Kim, S. Ahn, K.J. Kim, S. Jeon, D.-K. Lim, J.K. Kim, U. Kim, H.-N. Im, B. Koo, K.T. Lee, W. Jung, An universal oxygen electrode for reversible solid oxide electrochemical cells at reduced temperatures, Energy Environ. Sci. 16 (2023) 3803–3814, https://doi.org/10.1039/D2EE04108A.

[25] J. Yi, M. Schroeder, T. Weirich, J. Mayer, Behavior of $Ba(Co, Fe, Nb)O_{3-\delta}$ perovskite in CO_2 -containing atmospheres: degradation mechanism and materials design, Chem. Mater. 22 (2010) 6246–6253, https://doi.org/10.1021/cm101665r.

[26] J.H. Kim, J.K. Kim, H.G. Seo, D. Lim, S.J. Jeong, J. Seo, J. Kim, W. Jung, Ex-solved Ag nanocatalysts on a Sr-free parent scaffold authorize a highly efficient route of oxygen reduction, Adv. Funct. Mater. 30 (2020) 2001326, https://doi.org/10.1002/adfm.202001326.

[27] E. Quattrocchi, T.H. Wan, A. Belotti, D. Kim, S. Pepe, S.V. Kalinin, M. Ahmadi, F. Ciucci, The deep-DRT: a deep neural network approach to deconvolve the distribution of relaxation times from multidimensional electrochemical impedance spectroscopy data, Electrochim. Acta 392 (2021) 139010, https://doi.org/10.1016/j.electacta.2021.139010.

[28] M. Liang, Y. Wang, Y. Song, D. Guan, J. Wu, P. Chen, A. Maradesa, M. Xu, G. Yang, W. Zhou, W. Wang, R. Ran, F. Ciucci, Z. Shao, High-temperature water oxidation activity of a perovskite-based nanocomposite towards application as air electrode in reversible protonic ceramic cells, Appl. Catal. B Environ. 331 (2023) 122682, https://doi.org/10.1016/j.apcatb.2023.122682.

[29] Y.-M. Kim, J. He, M.D. Biegalski, H. Ambaye, V. Lauter, H.M. Christen, S. T. Pantelides, S.J. Pennycook, S.V. Kalinin, A.Y. Borisevich, Probing oxygen vacancy concentration and homogeneity in solid-oxide fuel-cell cathode materials on the subunit-cell level, Nat. Mater. 11 (2012) 888–894, https://doi.org/10.1038/nmat3393.

[30] X. Xu, H. Wang, J. Ma, W. Liu, X. Wang, M. Fronzi, L. Bi, Impressive performance of proton-conducting solid oxide fuel cells using a first-generation cathode with tailored cations, J. Mater. Chem. A 7 (2019) 18792–18798, https://doi.org/10.1039/C9TA06676D.

[31] Z. Zhang, Y. Zhu, Y. Zhong, W. Zhou, Z. Shao, Anion doping: a new strategy for developing high-performance perovskite-type cathode materials of solid oxide fuel cells, Adv. Energy Mater. 7 (2017) 1700242, https://doi.org/10.1002/aenm.201700242.

[32] Y. Zhang, J. Li, H. Xie, Z. Liu, S. Shen, Y. Teng, D. Guan, S. Zhai, Y. Song, W. Zhou, B. Chen, M. Ni, Z. Shao, CO_2-induced reconstruction for ORR-enhanced solid oxide fuel cell cathode, Chem. Eng. J. 462 (2023) 142216, https://doi.org/10.1016/j.cej.2023.142216.

[33] C. Zhou, X. Wang, D. Liu, M. Fei, J. Dai, D. Guan, Z. Hu, L. Zhang, Y. Wang, W. Wang, R. O'Hayre, S.P. Jiang, W. Zhou, M. Liu, Z. Shao, New strategy for boosting cathodic performance of protonic ceramic fuel cells through incorporating a superior hydronation second phase, Energy Environ. Mater. (2023) e12660, https://doi.org/10.1002/eem2.12660.

[34] R. Manabe, S.Ø. Stub, T. Norby, Y. Sekine, Evaluating surface protonic transport on cerium oxide via electrochemical impedance spectroscopy measurement, Solid State Commun. 270 (2018) 45–49, https://doi.org/10.1016/j.ssc.2017.11.010.

[35] C. Zhou, J. Sunarso, Y. Song, J. Dai, J. Zhang, B. Gu, W. Zhou, Z. Shao, New reduced-temperature ceramic fuel cells with dual-ion conducting electrolyte and triple-conducting double perovskite cathode, J. Mater. Chem. A 7 (2019) 13265–13274, https://doi.org/10.1039/C9TA03501J.

[36] X. Wang, W. Li, C. Zhou, M. Xu, Z. Hu, C.-W. Pao, W. Zhou, Z. Shao, Enhanced proton conduction with low oxygen vacancy concentration and favorable hydration for protonic ceramic fuel cells cathode, ACS Appl. Mater. Interfaces 15 (2023) 1339–1347, https://doi.org/10.1021/acsami.2c19343.

[37] K. Kreuer, Aspects of the formation and mobility of protonic charge carriers and the stability of perovskite-type oxides, Solid State Ion. 125 (1999) 285–302, https://doi.org/10.1016/S0167-2738(99)00188-5.

[38] K.T. Lee, A. Manthiram, Characterization of $Nd_{0.6}Sr_{0.4}Co_{1-y}Fe_yO_{3-\delta}$ ($0 \leq y \leq 0.5$) cathode materials for intermediate temperature solid oxide fuel cells, Solid State Ion. 176 (2005) 1521–1527, https://doi.org/10.1016/j.ssi.2005.05.002.

[39] R. Ren, Z. Wang, C. Xu, W. Sun, J. Qiao, D.W. Rooney, K. Sun, Tuning the defects of the triple conducting oxide $BaCo_{0.4}Fe_{0.4}Zr_{0.1}Y_{0.1}O_{3-\delta}$ perovskite toward enhanced cathode activity of protonic ceramic fuel cells, J. Mater. Chem. A 7 (2019) 18365–18372, https://doi.org/10.1039/C9TA04335G.

[40] F. Wang, T. Nakamura, K. Yashiro, J. Mizusaki, K. Amezawa, Effect of Nb doping on the chemical stability of BSCF-based solid solutions, Solid State Ion. 262 (2014) 719–723, https://doi.org/10.1016/j.ssi.2014.01.045.

[41] Y. Qiu, H. Li, Y. Liu, B. Chi, J. Pu, J. Li, Effects of niobium doping on the stability of $SrCo_{0.2}Fe_{0.8}O_{3-\delta}$ cathodes for intermediate temperature solid oxide fuel cells, J. Alloy. Compd. 829 (2020) 154503, https://doi.org/10.1016/j.jallcom.2020.154503.

[42] Y. Zhu, J. Sunarso, W. Zhou, S. Jiang, Z. Shao, High-performance $SrNb_{0.1}Co_{0.9-x}Fe_xO_{3-\delta}$ perovskite cathodes for low-temperature solid oxide fuel cells, J. Mater. Chem. A 2 (2014) 15454–15462, https://doi.org/10.1039/C4TA03208J.

[43] Y.-L. Huang, A.M. Hussain, E.D. Wachsman, Nanoscale cathode modification for high performance and stable low-temperature solid oxide fuel cells (SOFCs), Nano Energy 49 (2018) 186–192, https://doi.org/10.1016/j.nanoen.2018.04.028.

[44] H. Zhao, N. Xu, Y. Cheng, W. Wei, N. Chen, W. Ding, X. Lu, F. Li, Investigation of mixed conductor $BaCo_{0.7}Fe_{0.3-x}Y_xO_{3-\delta}$ with high oxygen permeability, J. Phys. Chem. C 114 (2010) 17975–17981, https://doi.org/10.1021/jp106220z.

[45] Y. Zhang, B. Chen, D. Guan, M. Xu, R. Ran, M. Ni, W. Zhou, R. O'Hayre, Z. Shao, Thermal-expansion offset for high-performance fuel cell cathodes, Nature 591 (2021) 246–251, https://doi.org/10.1038/s41586-021-03264-1.

[46] M. Arnold, H. Wang, A. Feldhoff, Influence of CO_2 on the oxygen permeation performance and the microstructure of perovskite-type $(Ba_{0.5}Sr_{0.5})(Co_{0.8}Fe_{0.2})O_{3-\delta}$ membranes, J. Membr. Sci. 293 (2007) 44–52, https://doi.org/10.1016/j.memsci.2007.01.032.

[47] X. Wang, M. Fei, C. Zhou, W. Li, X. Wang, X. Shen, D. Liu, W. Chen, P. Chen, G. Jiang, R. Ran, W. Zhou, Enhanced proton conductivity and CO_2-tolerance of intermediate-temperature protonic ceramic fuel cell with lanthanum tungstate-based composite cathode, Compos. Part B Eng. 253 (2023) 110565, https://doi.org/10.1016/j.compositesb.2023.110565.

[48] N.C. Jeong, J.S. Lee, E.L. Tae, Y.J. Lee, K.B. Yoon, Acidity scale for metal oxides and sanderson's electronegativities of lanthanide elements, Angew. Chem. Int. Ed. 47 (2008) 10128–10132, https://doi.org/10.1002/anie.200803837.

[49] C. Zhou, D. Liu, M. Fei, X. Wang, R. Ran, M. Xu, W. Wang, W. Zhou, R. O'Hayre, Z. Shao, Cathode water management towards improved performance of protonic ceramic fuel cells, J. Power Sources 556 (2023) 232403, https://doi.org/10.1016/j.jpowsour.2022.232403.

[50] C. Berger, E. Bucher, R. Merkle, C. Nader, J. Lammer, W. Grogger, J. Maier, W. Sitte, Influence of Y-substitution on phase composition and proton uptake of self-generated $Ba(Ce,Fe)O_{3-\delta}$ –$Ba(Fe,Ce)O_{3-\delta}$ composites, J. Mater. Chem. A 10 (2022) 2474–2482, https://doi.org/10.1039/D1TA07208K.

[51] D. Poetzsch, R. Merkle, J. Maier, Proton uptake in the H^+-SOFC cathode material $Ba_{0.5}Sr_{0.5}Fe_{0.8}Zn_{0.2}O_{3-\delta}$: transition from hydration to hydrogenation with increasing oxygen partial pressure, Faraday Discuss. 182 (2015) 129–143, https://doi.org/10.1039/C5FD00013K.